

## Supplementary Information

### **Herringbone Packed Contorted Aromatics with Ordered Three-dimensional Channels as Fast-charging and Low-temperature Lithium-ion Battery Anode**

Lei Yang<sup>a†</sup>, Xin Zhu<sup>a†</sup>, Qinghai Zhou<sup>a</sup>, Chaoran Qi<sup>a</sup>, Qiyu Wang<sup>b</sup>, Fengchun Shi<sup>b</sup>, Meng Zhu<sup>b</sup>, Guorong Chen<sup>b</sup>, Dongdong Wang<sup>c</sup>, Xiaoyan Liu<sup>\*a</sup>, Liwei Wang<sup>\*a</sup>, Dongsong Zhang<sup>\*b</sup>, Hexing Li<sup>\*a</sup>, Shengxiong Xiao<sup>\*a</sup>

<sup>a</sup> The Education Ministry Key Lab of Resource Chemistry, Joint International Research Laboratory of Resource Chemistry, Ministry of Education, Shanghai Key Laboratory of Rare Earth Functional Materials, Shanghai Non-carbon Energy Conversion and Utilization Institute, College of Chemistry and Materials Science, Shanghai Normal University, Shanghai 200234, P. R. China

<sup>b</sup> Department of Chemistry, Research Center of Nano Science and Technology, College of Sciences, Shanghai University, Shanghai 200444, P. R. China.

<sup>c</sup> Key Laboratory of Colloid and Interface Chemistry, Ministry of Education, School of Chemistry and Chemical Engineering, Shandong University, Jinan 250100, P. R. China

E-mail: xiaosx@shnu.edu.cn, hexing-li@shnu.edu.cn, dszhang@shu.edu.cn, wangliwei@shnu.edu.cn, xyliu@shnu.edu.cn

†These authors contributed equally to this work.

## Experimental Section

**Material characterizations.**  $^1\text{H}$  nuclear magnetic resonance (NMR) and  $^{13}\text{C}$  NMR spectra were collected using a Bruker DRX400 spectrometer operating at 400 MHz at 298 K. High resolution mass spectra (HRMS) were performed using a Bruker solanX 70 FT-MS. Thermal gravimetric analysis (TGA) measurements were performed on a Discovery TGA under air and argon at a heating rate of 10 °C/min. The single-crystal X-ray diffraction (XRD) was performed on a Bruker smart Apex. The powder X-ray diffraction (PXRD) was measured on an Ultima IV Powder X-ray diffractometer. The scanning electron microscopy (SEM) images were collected using a JSM-6380LV. The transmission electron microscopy (TEM) images were collected using a TALOS F200S. The Fourier-transform infrared (FT-IR) spectra were measured with Nicoletis50. The Raman spectra were measured with LABRAM. The X-ray photoelectron spectroscopy (XPS) was performed using a Thermo Scientific K-lpha. The in-situ FTIR was measured with Nicolet 6700. The in-situ Raman was measured with LabRAM HR Evolution.

**Preparation of electrodes and electrochemical test.** The working electrodes were prepared by *c*-HBC-80@G or *c*-OBCB-80@G samples (80 wt%) with Super P (10 wt%) and poly(vinylidene fluoride) (PVDF) (10 wt%) in *N*-methyl-2-pyrrolidone (NMP) to form a homogenous slurry. Then, they were casted onto a Cu film with an areal active material loading of 1 mg cm<sup>-2</sup>. After drying at 100 °C for 12 hours in a vacuum oven, the electrodes were cut into disks with dimeters of 12 mm. CR2032-type coin cells were assembled in an Ar-filled glove box with Celgard 2400 membrane as separator and lithium chips as counter/reference electrodes. The electrolyte used at 25 °C was 1.0 M LiPF<sub>6</sub> in ethylene carbonate (EC) and dimethyl carbonate (DMC) mixture (1: 1 in volume) with 5% FEC. The electrolyte at -20 °C was 1.0 M LiTFSI in DOL and DME mixture (1: 1 in volume) with 1% LiNO<sub>3</sub>. The *c*-HBC-80@G anodes was first pre-cycled to form the SEI in advance before the full cell was prepared. The negative/positive electrode capacity ratio of the full cell was 1.1. The full cell was

cycled between 1.1V and 3.8 V. Galvanostatic tests were performed by Wuhan Land Test System (CT3002A, LAND) at various current densities with voltage cutoff of 0.01-3.00 V. Besides, cycling test at 5 A g<sup>-1</sup> of *c*-HBC-8O@G and *c*-OBCB-8O@G electrodes were first activated at the current density of 125 mA g<sup>-1</sup> for 20 cycles. The electrodes for *in situ* FT-IR test and *in situ* Raman test were consisted of 90 wt% *c*-HBC-8O and 10 wt% PVDF binder. Cyclic voltammetry (CV) and electrochemical impedance spectroscopy (EIS) were conducted by BioLogic (VSP-300).

**Computational Details.** The theoretical calculations were performed via the Gaussian 16 suite<sup>1</sup> of programs. Geometry optimization of the molecules were performed by the B3LYP functional and 6-31G(d) basis set<sup>2</sup>. The free energy of the molecules and these molecules with Li atoms were estimated at B3LYP /6-311+G(d, p) level of theory. The vibrational frequencies of the optimized structures were carried out at B3LYP / 6-311+G(d, p) level. Computed structures were illustrated using CYLView<sup>3</sup>. The Visual Molecular Dynamics (VMD)<sup>4</sup> program was used to plot the color-filled isosurfaces graphs to visualize the ESP of *c*-HBC-8O with Li atoms.

### Synthesis of *c*-HBC-8O and *c*-OBCB-8O

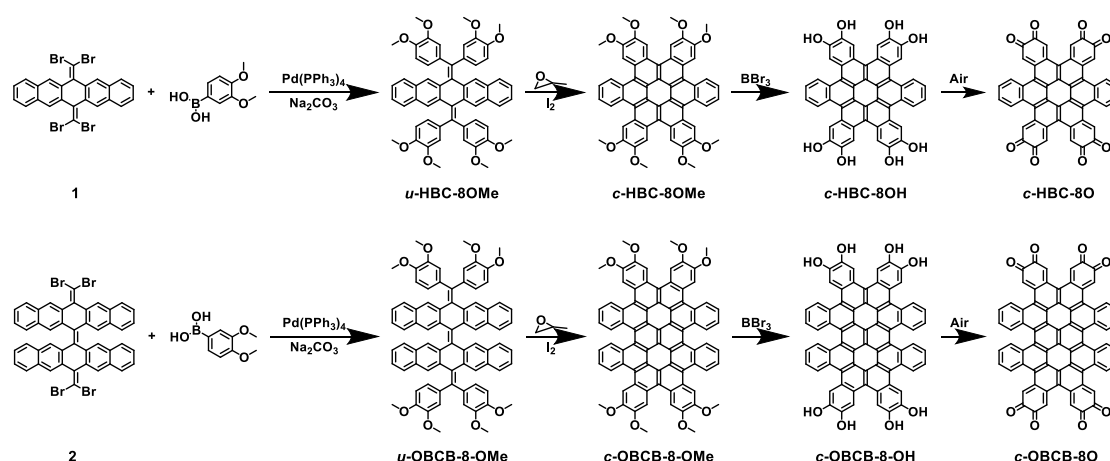


**Figure S1.** Synthetic routes of *c*-HBC-8O and *c*-OBCB-8O.

## 4. Experimental Section/Methods

Compound **1** and compound **2** were synthesized according to the reported procedure<sup>5, 6</sup>. Other reagents were obtained from commercial suppliers such as Adamas<sup>®</sup> and Aladdin Reagent Inc. without further purification.

*Synthesis of octamethoxy uncyclized HBC (u-HBC-8-OMe):* 6,13-bis(dibromomethylene)-6,13-dihydropentacene (compound **1**) (1 g, 1.61 mmol), (3,4-dimethoxyphenyl) boronic acid (1.76 g, 9.68 mmol), Na<sub>2</sub>CO<sub>3</sub> (1.37 g, 12.90 mmol) and Pd (PPh<sub>3</sub>)<sub>4</sub> (11.32 mg, 0.016 mmol) were accurately weighed into a 50 mL Shrek flask, toluene (20 mL), CH<sub>3</sub>OH (5 mL) and H<sub>2</sub>O (5 mL) were added, and the reaction was heated to 90 °C for 24 hours in a nitrogen environment. After the reaction was over, it was cooled to room temperature and distilled at reduced pressure to remove organic solvent. The residue was extracted with dichloromethane for three times, and the organic phase was combined. The organic phase was dried with anhydrous sodium sulfate, and the solvent was removed by vacuum distillation. *u*-HBC-8-OMe was isolated via column chromatography using dichloromethane: petroleum ether = 4: 1 as the eluent to yield a white solid 1.1 g (yield 81%). <sup>1</sup>H NMR (400 MHz, Chloroform-*d*) δ=7.64 (s, 4H), 7.42 (dd, *J* = 6.2, 3.3 Hz, 4H), 7.24 (dd, *J* = 6.2, 3.2 Hz, 4H), 6.97 (d, *J* = 7.3 Hz, 4H), 6.74 (d, *J* = 8.3 Hz, 4H), 3.83 (s, 12H), 3.63 (s, 12H). <sup>13</sup>C NMR (100 MHz, Chloroform-*d*) δ=148.42, 147.95, 139.63, 136.37, 135.14, 134.76, 131.46, 127.70, 126.70, 125.68, 122.65, 113.97, 110.79, 77.37, 77.06, 76.74, 56.03, 55.82. HRMS (APCI) calculated *m/z* for [C<sub>56</sub>H<sub>48</sub>O<sub>8</sub> + H]<sup>+</sup>: 849.3421, found: 849.3423.

*Synthesis of octamethoxy contorted HBC (c-HBC-8OMe):* *u*-HBC-8-OMe (500 mg, 0.59 mmol) was weighed and dissolved in anhydrous toluene (250 mL), then iodine (717.49 mg, 2.83 mmol) and epoxy-propane (5 mL) were added. After purging with nitrogen for 30 min, the solution was subjected to a medium pressure mercury UV lamp for 12 h in nitrogen environment. A large amount of yellow solid was produced after 12 h, and the solvent was removed by vacuum pumping. Filtration and washing with small amounts of methanol and hexanes to obtain a yellow solid, 455.4 mg (yield 92%). <sup>1</sup>H NMR (400 MHz, Chloroform-*d*) δ=9.34 (dd, *J* = 6.3, 3.4 Hz, 4H), 8.75 (d, *J* =

10.5 Hz, 8H), 7.81 (dd,  $J = 6.4, 3.3$  Hz, 4H), 4.27 – 4.16 (m, 24H).  $^{13}\text{C}$  NMR (100 MHz, Chloroform- $d$ )  $\delta$ =148.61, 148.43, 129.75, 128.14, 126.01, 125.26, 125.05, 124.87, 124.25, 120.98, 119.98, 109.75, 108.69, 77.36, 77.04, 76.73, 56.21, 56.16. HRMS (APCI) calculated  $m/z$  for  $[\text{C}_{56}\text{H}_{40}\text{O}_8 + \text{H}]^+$ : 841.2796, found: 847.2791.

*Synthesis of octahydroxy contorted HBC (c-HBC-8OH)*: A mixture of *c*-HBC-8OMe (1 g, 1.19 mmol) and DCM (100 mL) was cooled to 0 °C.  $\text{BBr}_3$  (5.96 g, 23.78 mol) was then added dropwise, and the mixture was refluxed for 2 h. Excess boron tribromide was quenched by the slow addition of ice water. The mixture was filtered to yield a green solid, 0.77 g (yield 89%).  $^1\text{H}$  NMR (400 MHz,  $\text{DMSO-}d_6$ )  $\delta$ =9.97 (s, 4H), 9.87 (s, 4H), 9.19 (dd,  $J = 6.3, 3.5$  Hz, 4H), 8.57 (d,  $J = 9.9$  Hz, 8H), 7.84 (dd,  $J = 6.4, 3.3$  Hz, 4H).  $^{13}\text{C}$  NMR (100 MHz,  $\text{DMSO-}d_6$ )  $\delta$ =146.86, 146.71, 146.47, 129.31, 128.41, 126.39, 124.81, 124.55, 124.50, 123.07, 120.06, 118.13, 113.06, 112.84, 56.51, 56.01, 40.63, 40.58, 40.42, 40.37, 40.17, 39.95, 39.75, 39.54, 39.33, 19.04. HRMS (APCI) calculated  $m/z$  for  $[\text{C}_{48}\text{H}_{24}\text{O}_8 + \text{H}]^+$ : 729.1544, found: 729.1535.

*Synthesis of contorted HBC octa-ketone (c-HBC-8O)*: *c*-HBC-8OH (0.5 g) was weighed in a quartz boat and was heated to 150 °C in air for 15 h. After the reaction, dichloromethane, methanol and tetrahydrofuran were used to wash the solid material through a Soxhlet extractor to obtain *c*-HBC-8O, 0.41 g (yield 82%). HRMS (APCI) calculated  $m/z$  for  $[\text{C}_{48}\text{H}_{16}\text{O}_8 + \text{H}]^+$ : 721.0918, found: 721.0396.

*Synthesis of octamethoxy uncyclized OBCB (u-OBCB-8-OMe)*: compound **2** (1 g, 1.12 mmol), (3,4-dimethoxyphenyl) boronic acid (0.97 g, 5.36 mmol),  $\text{Na}_2\text{CO}_3$  (0.95 g, 8.93 mmol) and  $\text{Pd}(\text{PPh}_3)_4$  (78.31 mg, 0.011 mmol) were accurately weighed into a 50 mL Shrek flask, toluene (30 mL),  $\text{CH}_3\text{OH}$  (6 mL) and  $\text{H}_2\text{O}$  (6 mL) were added, and the reaction was heated to 90 °C for 24 hours in a nitrogen environment. After the reaction was over, it was cooled to room temperature and distilled at reduced pressure to remove organic solvent. Dichloromethane was used to extract the organic phase for three times, and the organic phase was combined. The organic phase was dried with anhydrous sodium sulfate, and the solvent was removed by vacuum

distillation. *u*-OBCB-8-OMe was isolated via column chromatography as a white solid, 0.81 g (yield 64%). <sup>1</sup>H NMR (400 MHz, DMSO-*d*<sub>6</sub>) δ=7.88 (s, 4H), 7.67 (s, 4H), 7.63 (d, J = 8.2 Hz, 4H), 7.45 (d, J = 2.0 Hz, 4H), 7.40 (t, J = 7.5 Hz, 4H), 7.34 – 7.22 (m, 12H), 7.10 (d, J = 8.3 Hz, 4H), 3.84 (s, 24H). <sup>13</sup>C NMR (100 MHz, Chloroform-*d*) δ=148.94, 148.91, 148.28, 148.23, 140.03, 136.93, 136.91, 135.47, 135.16, 135.14, 133.51, 131.87, 131.17, 127.86, 127.67, 127.46, 126.79, 125.88, 125.83, 122.69, 122.66, 113.74, 113.62, 111.09, 111.03, 77.35, 77.03, 76.71, 56.44, 56.42, 55.94, 1.03. HRMS (APCI) calculated m/z for [C<sub>78</sub>H<sub>60</sub>O<sub>8</sub> + H]<sup>+</sup>: 1125.4361, found: 1125.4365.

*Synthesis of octamethoxy contorted OBCB (c-OBCB-8OMe)*: *u*-OBCB-8-OMe (500 mg, 0.44 mmol) was weighed and dissolved in 250 mL of anhydrous toluene, then iodine (789.40 mg, 3.11 mmol) and epoxy-propane (5 mL) were added. After purging with nitrogen for 30 min, the solution was subjected to a medium pressure mercury UV lamp for 12 h in nitrogen environment. A large amount of yellow solid was produced after 12 h light, and the solvent was removed by vacuum pumping. Filtration and washing small amounts of methanol hexanes to obtain a red solid, 310 mg (yield 63%). <sup>1</sup>H NMR (400 MHz, Chloroform-*d*) δ=9.39 (d, J = 8.3 Hz, 4H), 9.19 (d, J = 8.4 Hz, 4H), 8.99 (d, J = 22.2 Hz, 8H), 7.77 (t, J = 7.6 Hz, 4H), 7.57 (t, J = 7.6 Hz, 4H), 4.32 (d, J = 24.5 Hz, 24H). <sup>13</sup>C NMR (100 MHz, Chloroform-*d*) δ=148.85, 148.70, 131.47, 130.65, 128.43, 128.08, 126.20, 125.39, 125.36, 125.18, 125.13, 123.56, 123.30, 121.00, 120.82, 120.73, 110.13, 108.89, 77.37, 77.05, 76.73, 56.43, 56.27. HRMS (APCI) calculated m/z for [C<sub>78</sub>H<sub>60</sub>O<sub>8</sub> + H]<sup>+</sup>: 1113.3422, found: 1113.3420.

*Synthesis of octahydroxy contorted OBCB (c-OBCB-8-OH)*: A mixture of *c*-OBCB-8OMe (1 g, 1.19 mmol), and DCM (150 mL) was cooled to 0 °C. BBr<sub>3</sub> (4.5 g (17.97 mol) was then added dropwise, and the mixture was refluxed for 2 h. Excess boron tribromide was quenched by the slow addition of ice water. The mixture was filtered to yield a deep red solid, 0.81 g (yield 90%). <sup>1</sup>H NMR (400 MHz, DMSO-*d*<sub>6</sub>) δ=10.17 (s, 4H), 10.11 (s, 4H), 9.28 (d, J = 8.3 Hz, 4H), 8.95 (d, J = 8.4 Hz, 4H), 8.82 (d, J = 16.7 Hz, 8H), 7.84 (t, J = 7.7 Hz, 4H), 7.61 (t, J = 7.7 Hz, 4H). <sup>13</sup>C NMR (100 MHz, DMSO-*d*<sub>6</sub>)

$\delta$ =147.25, 147.10, 130.89, 129.94, 128.79, 128.27, 127.14, 125.91, 125.09, 125.03, 124.69, 124.46, 123.12, 122.54, 120.43, 119.48, 118.63, 113.48, 113.02, 40.65, 40.60, 40.44, 40.39, 40.18, 39.97, 39.76, 39.55, 39.35. HRMS (APCI) calculated  $m/z$  for  $[C_{78}H_{60}O_8 + H]^+$ : 1001.2170, found: 1001.2158.

*Synthesis of contorted OBCB octa-ketone (c-OBCB-8O):* *c*-OBCB-8OH (0.5 g) was weighed in a quartz boat and was heated to 220 °C in air for 12 h. After the reaction, dichloromethane, methanol and tetrahydrofuran were used to wash the solid material through a Soxhlet extractor to obtain *c*-OBCB-8O, 0.44 g (yield 80%). HRMS (APCI) calculated  $m/z$  for  $[C_{70}H_{24}O_8 + Na]^+$ : 1015.1369, found: 1015.1282.

*Synthesis of c-HBC-8O@G:* *c*-HBC-8OH (0.8 g) was weighed and dissolved it in DMF (100 mL). Next, graphene (0.2 g) was added to the solution and was dispersed evenly. After achieving a homogeneous dispersion, the organic solvent was removed by vacuum distillation to obtain *c*-HBC-8OH@G. Heating *c*-HBC-8OH@G in air at 150 °C for 15 hours yielded *c*-HBC-8O@G as the final sample.

*Synthesis of c-OBCB-8O@G:* *c*-OBCB-8OH (0.8 g) was weighed and dissolved in DMF (100 mL). Next, graphene (0.2 g) was added to the solution and was dispersed evenly. After achieving a homogeneous dispersion, the organic solvent was removed by vacuum distillation to obtain *c*-OBCB-8OH@G. Heating *c*-OBCB-8OH@G in air at 220 °C for 12 hours yielded *c*-OBCB-8O@G as the final sample.

Material characterizations.

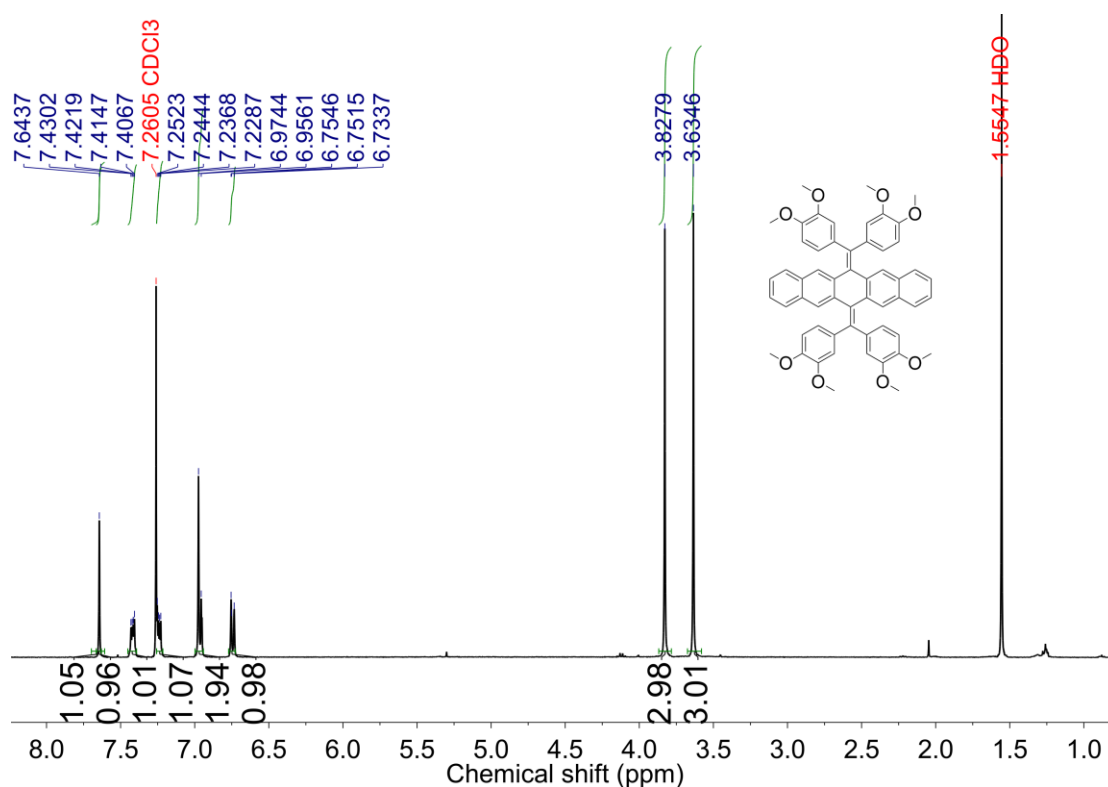


Figure S2. <sup>1</sup>H NMR spectrum of *u*-HBC-8-OMe (400 MHz, CDCl<sub>3</sub>, 298 K).

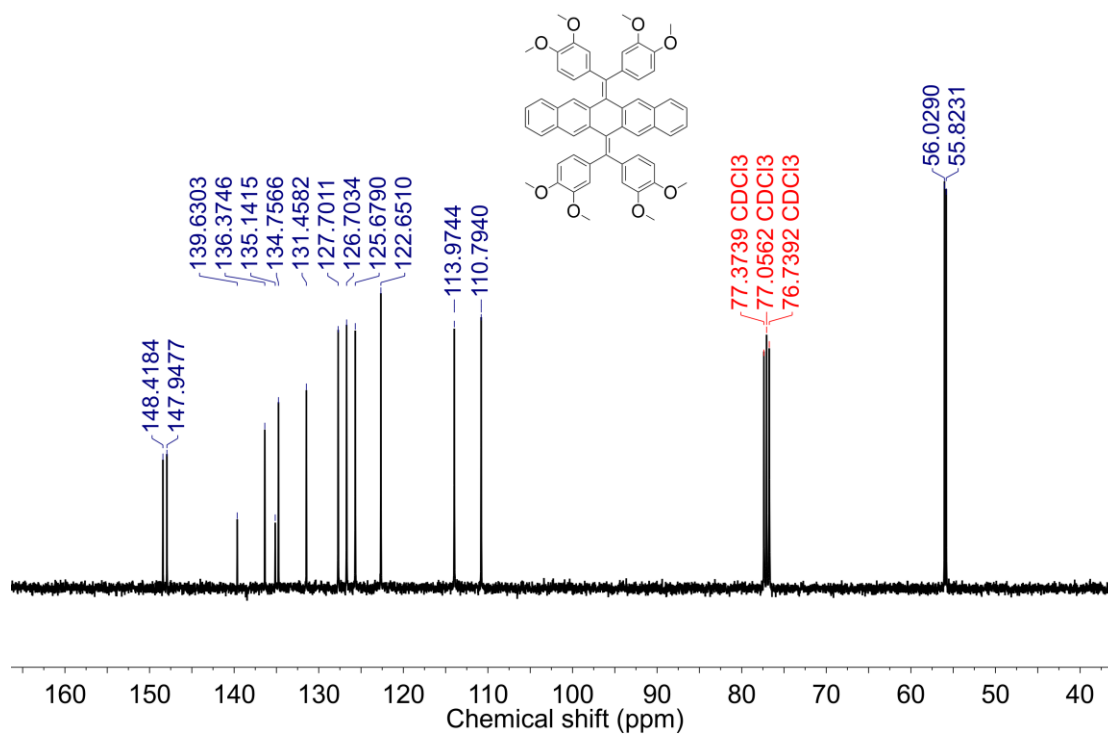
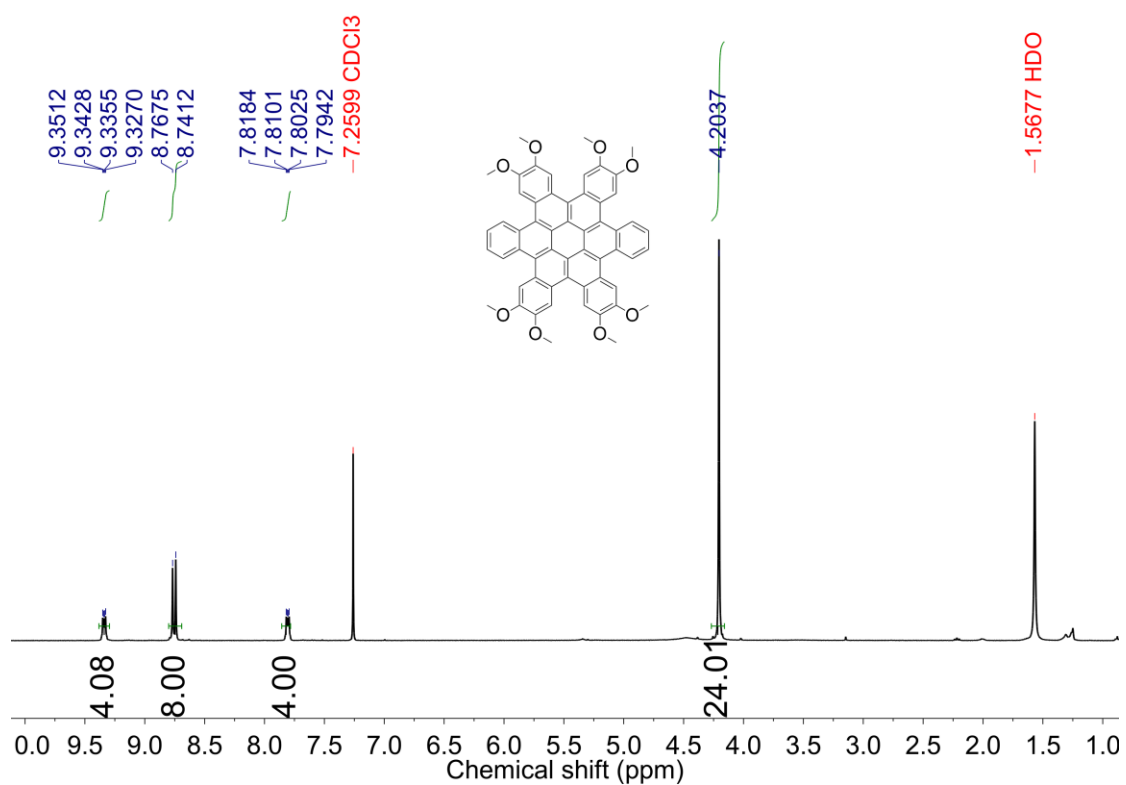
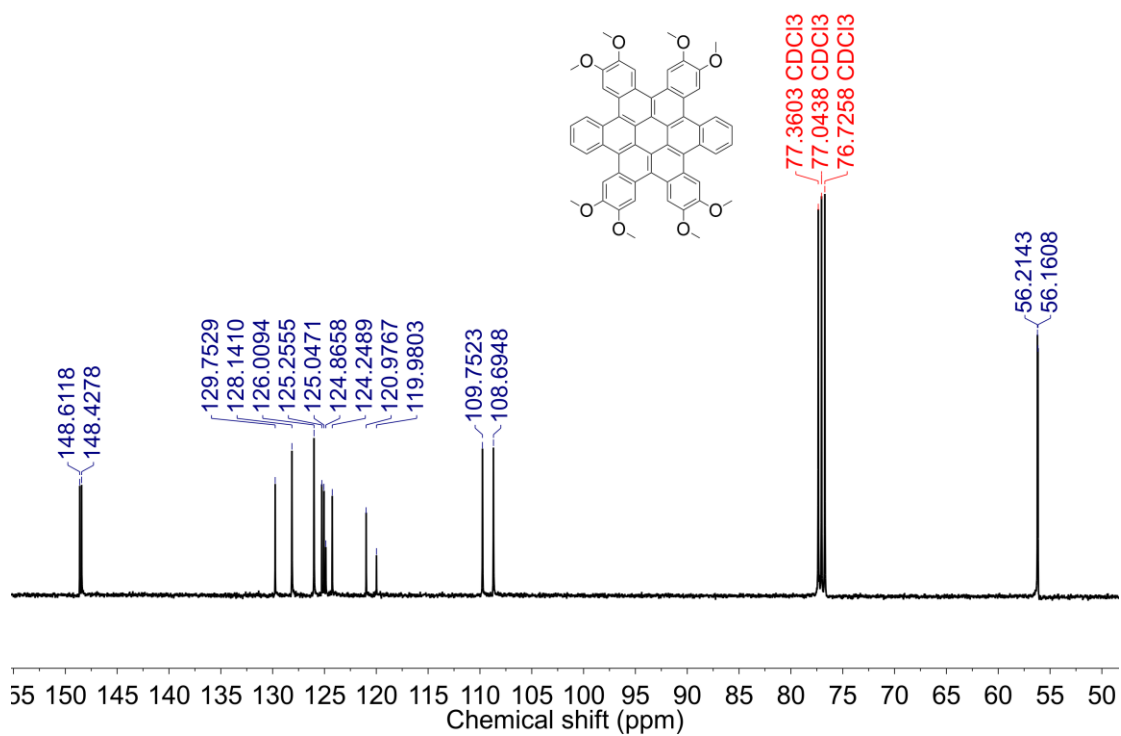


Figure S3. <sup>13</sup>C NMR spectrum of *u*-HBC-8-OMe (100 MHz, CDCl<sub>3</sub>, 298 K).

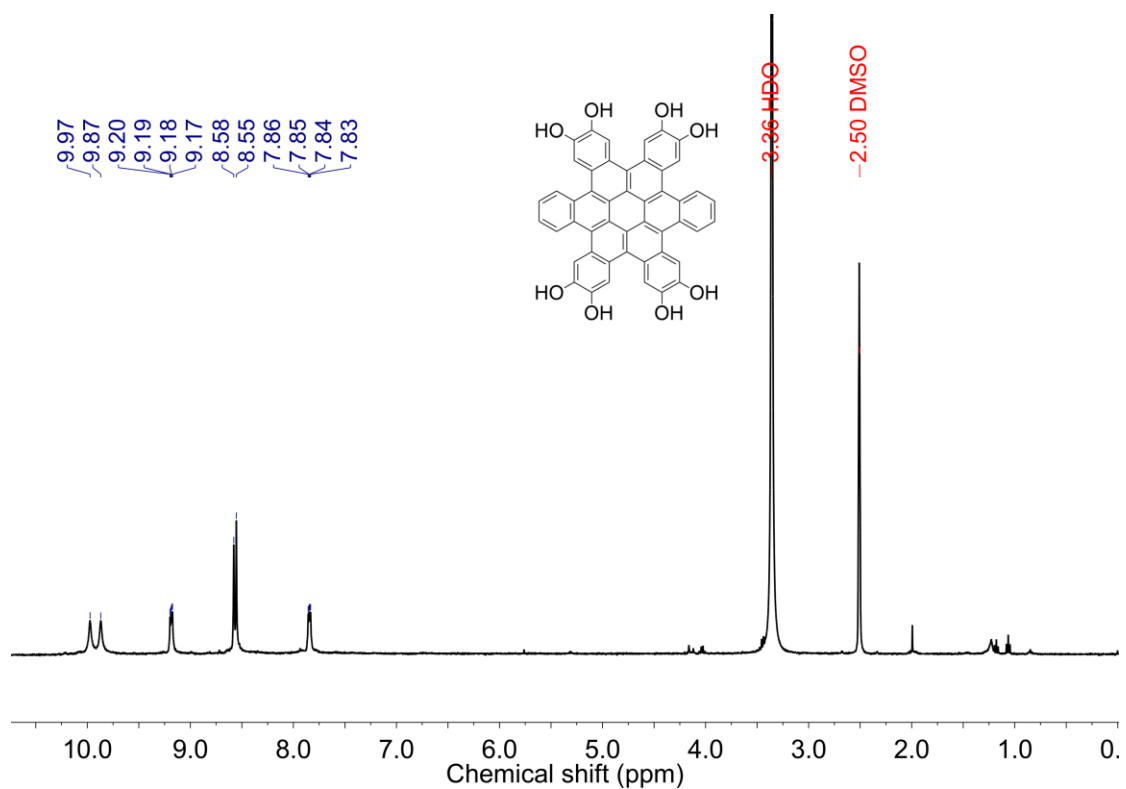




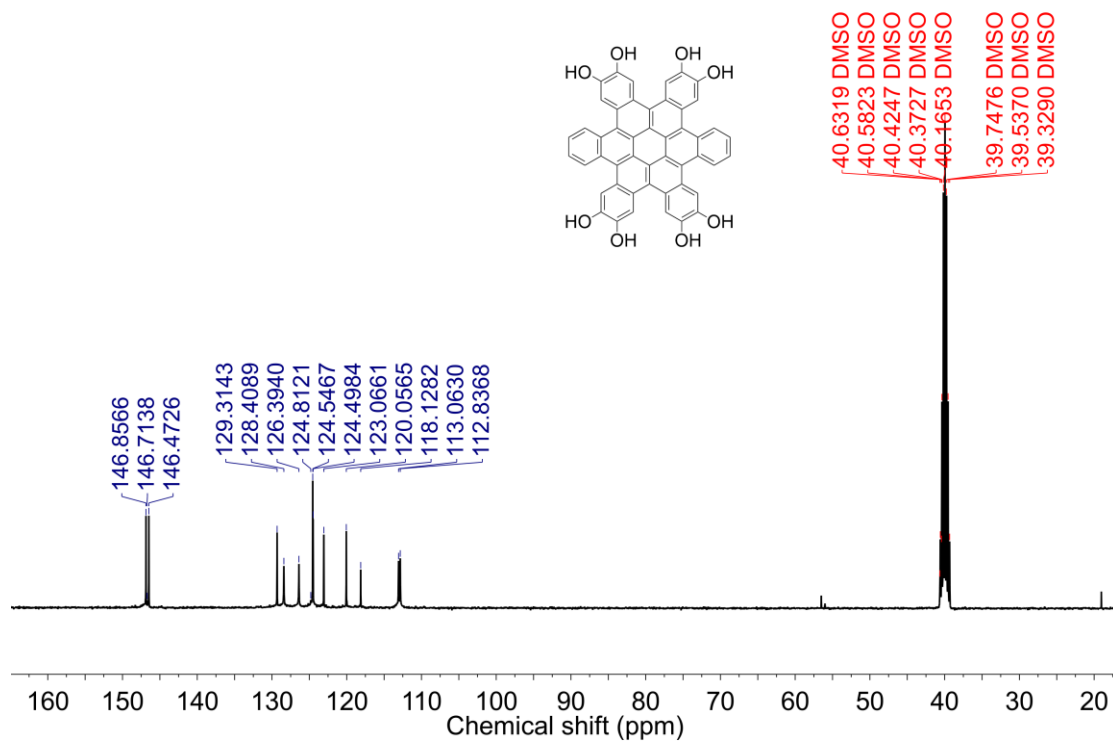
**Figure S4.** <sup>1</sup>H NMR spectrum of *c*-HBC-8OMe (400 MHz, CDCl<sub>3</sub>, 298 K).



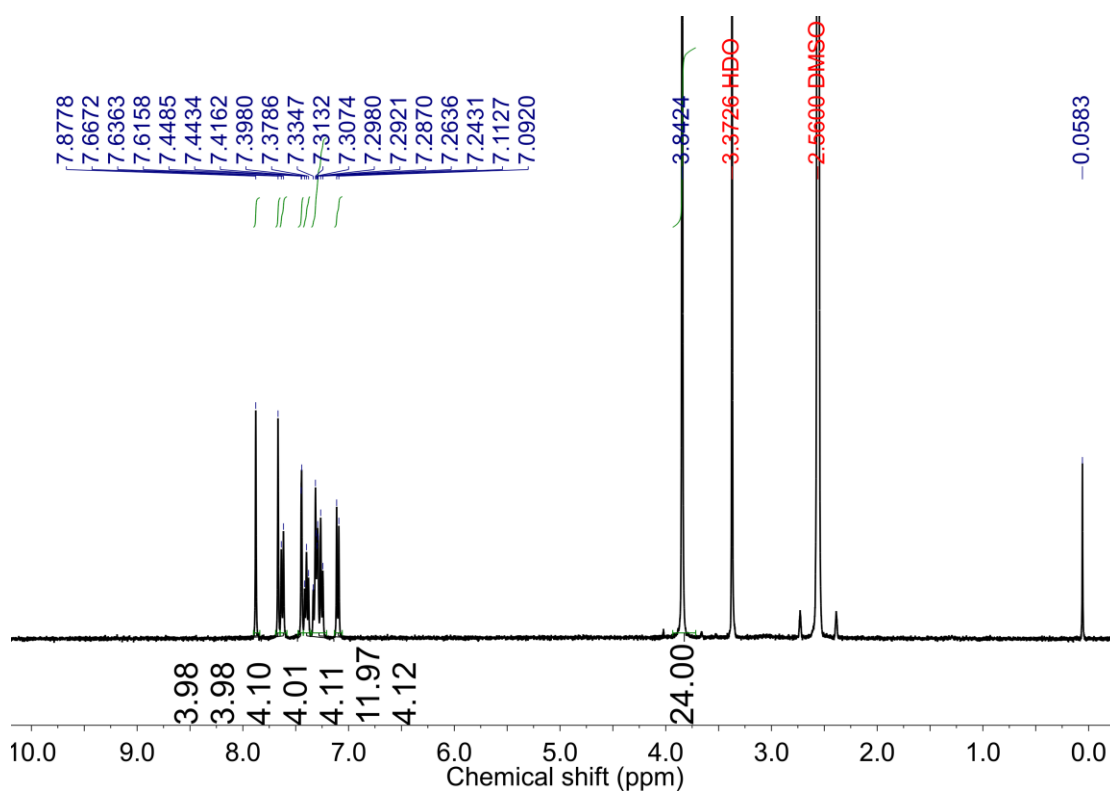
**Figure S5.** <sup>13</sup>C NMR spectrum of *c*-HBC-8OMe (100 MHz, CDCl<sub>3</sub>, 298 K).



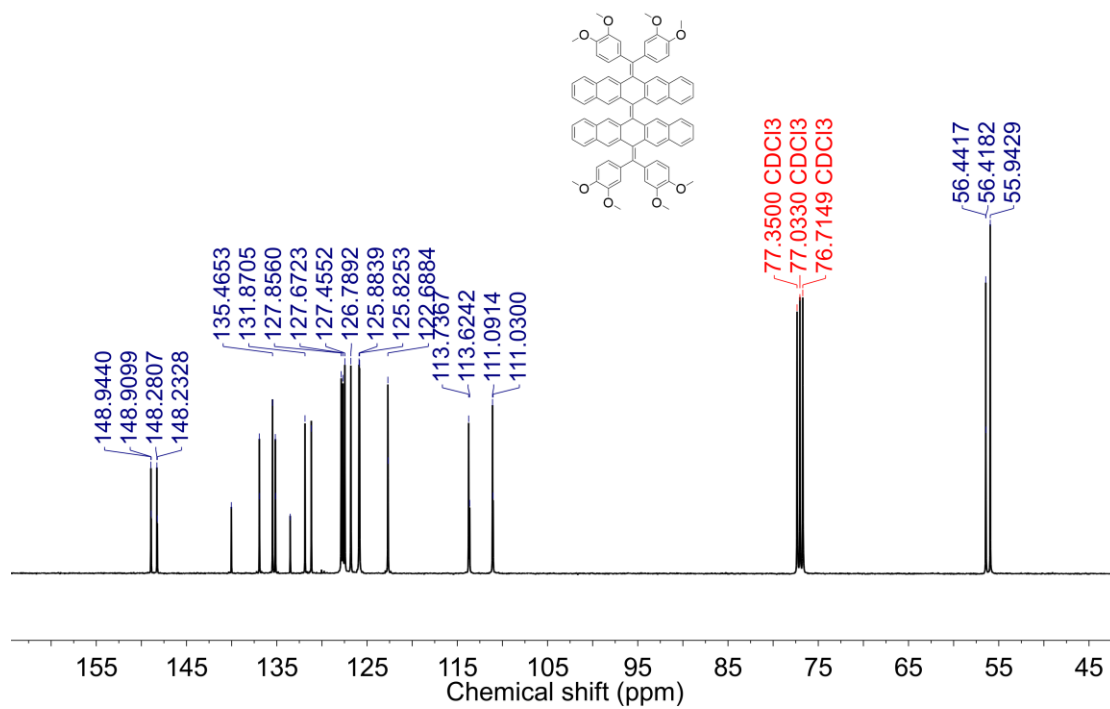
**Figure S6.** <sup>1</sup>H NMR spectrum of *c*-HBC-8OH (400 MHz, DMSO-*d*<sub>6</sub>, 298 K).



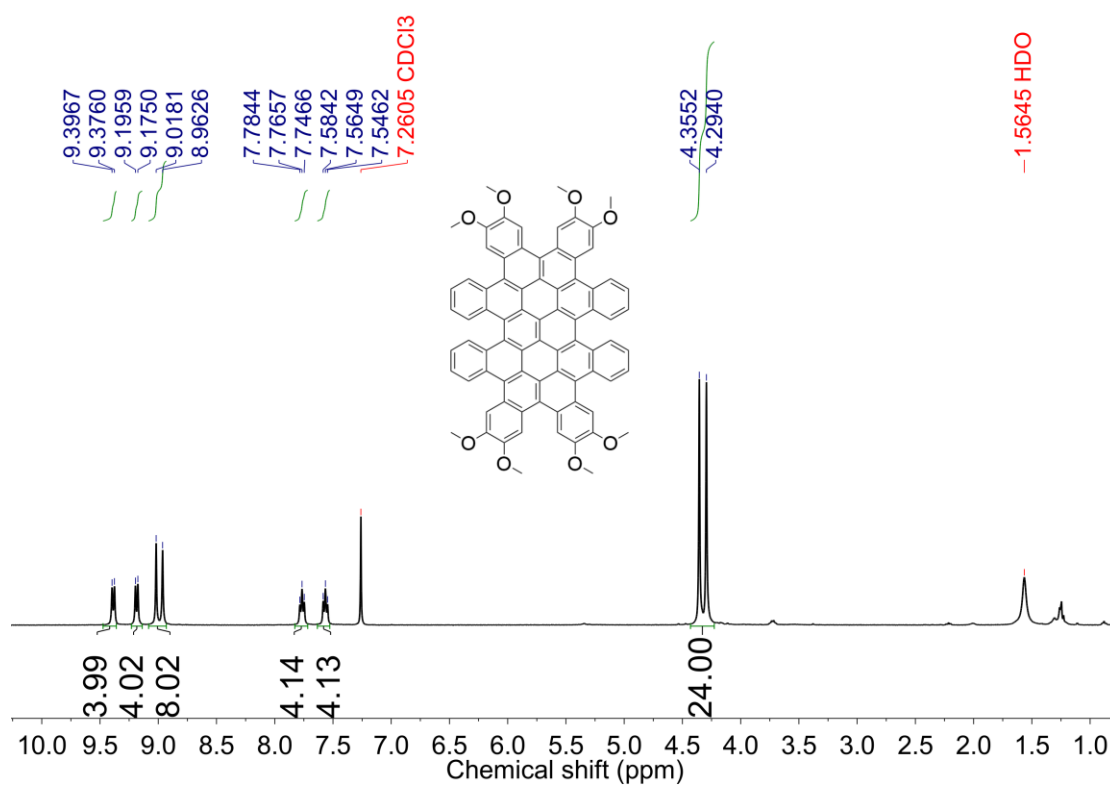
**Figure S7.** <sup>13</sup>C NMR spectrum of *c*-HBC-8OH (100 MHz, DMSO-*d*<sub>6</sub>, 298 K).



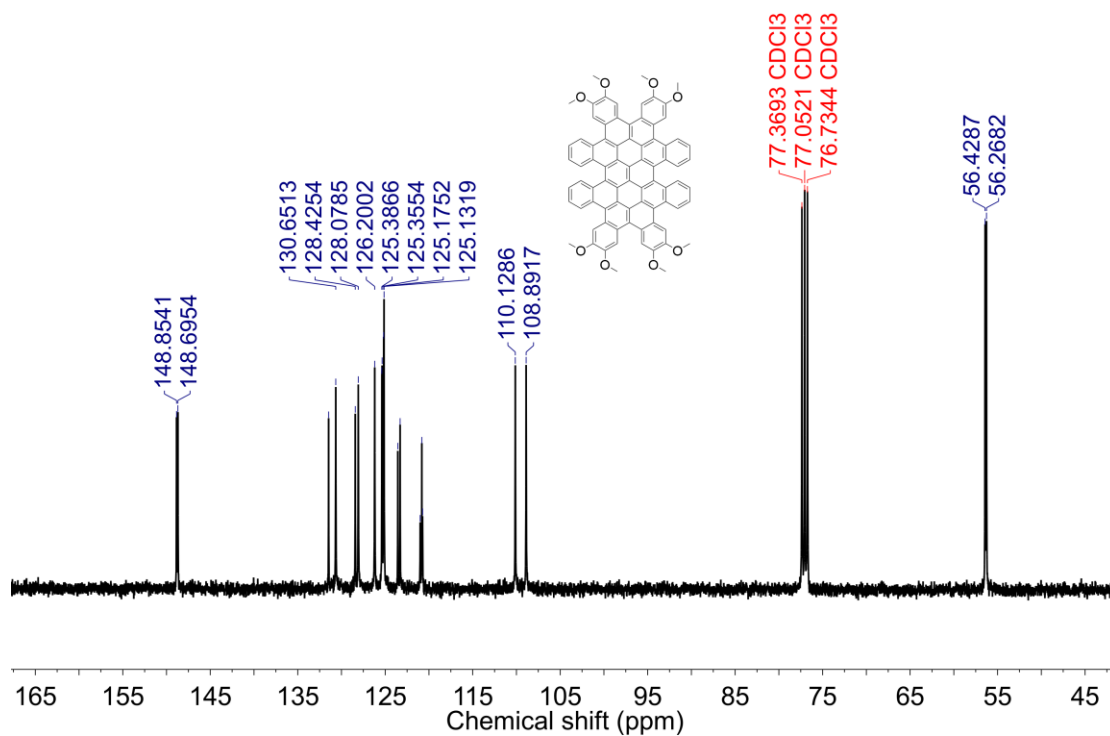
**Figure S8.**  $^1\text{H}$  NMR spectrum of *u*-OBCB-8-OMe (400 MHz,  $\text{DMSO-}d_6$ , 298 K).



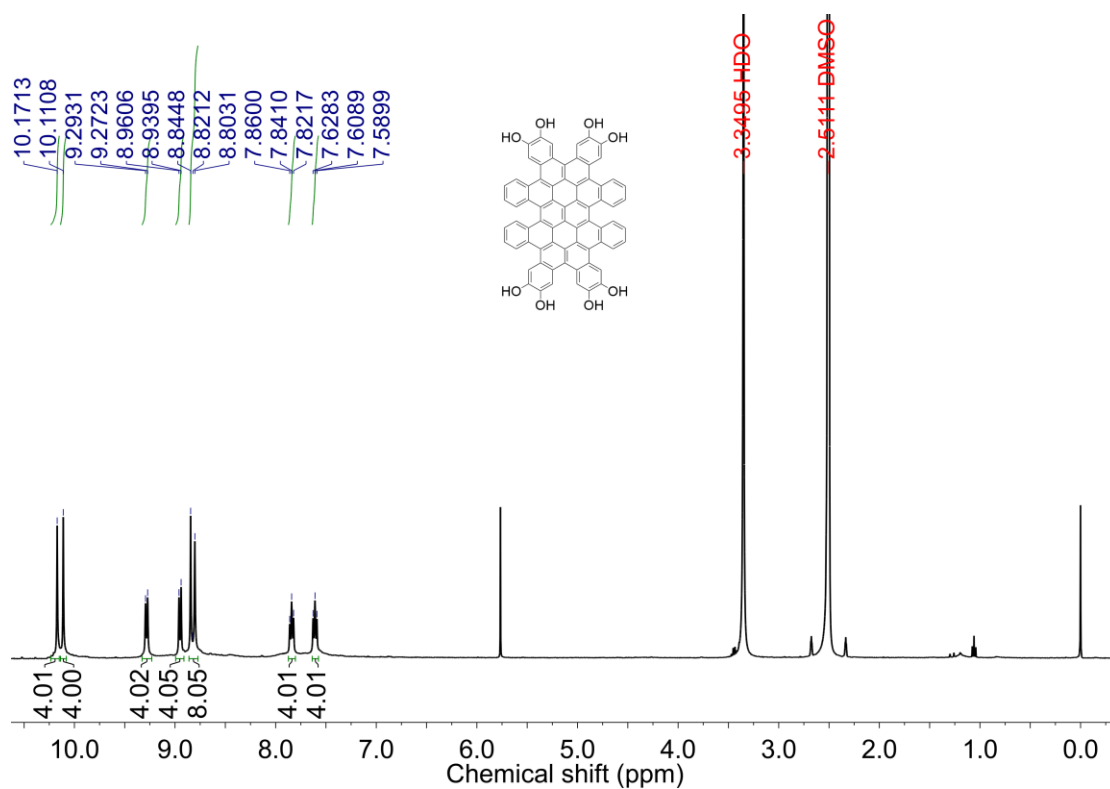
**Figure S9.**  $^{13}\text{C}$  NMR spectrum of *u*-OBCB-8-OMe (100 MHz,  $\text{CDCl}_3$ , 298 K).



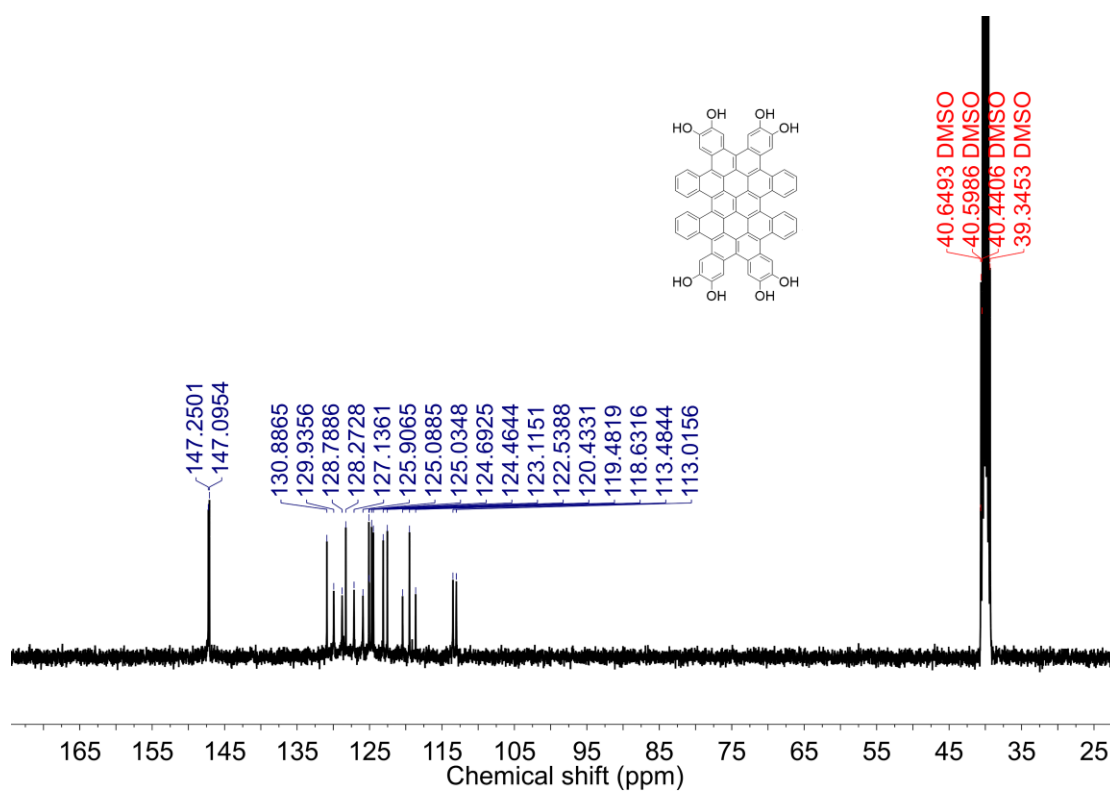
**Figure S10.** <sup>1</sup>H NMR spectrum of *c*-OBCB-8-OMe (400 MHz, CDCl<sub>3</sub>, 298 K).



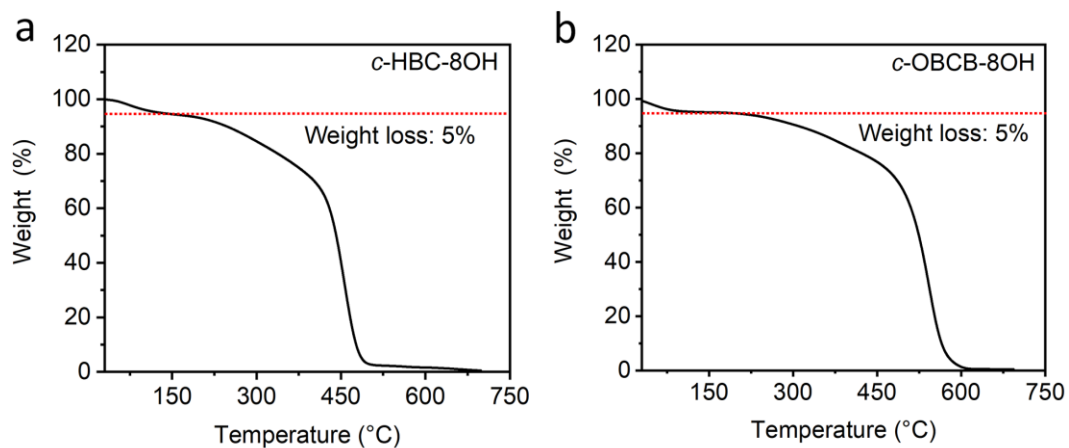
**Figure S11.** <sup>13</sup>C NMR spectrum of *c*-OBCB-8-OMe (100 MHz, CDCl<sub>3</sub>, 298 K).



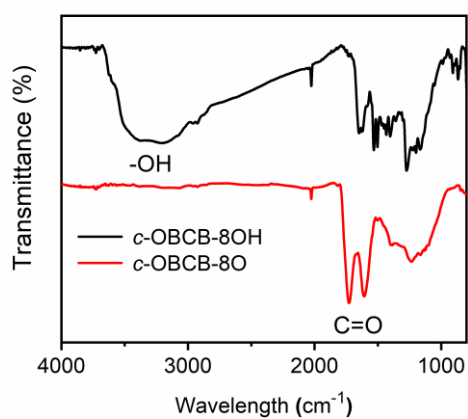
**Figure S12.**  $^1\text{H}$  NMR spectrum of *c*-OBCB-8-OH (400 MHz,  $\text{DMSO-}d_6$ , 298 K).



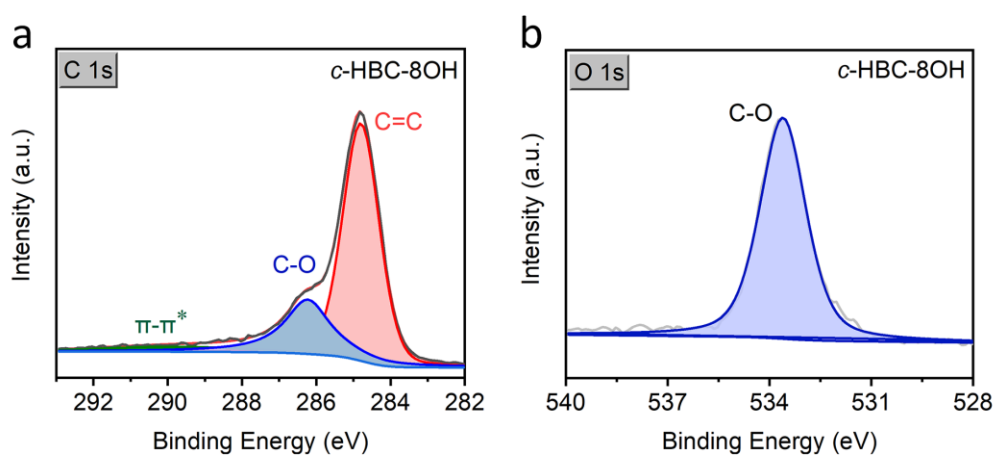
**Figure S13.**  $^{13}\text{C}$  NMR spectrum of *c*-OBCB-8-OH (100 MHz,  $\text{DMSO-}d_6$ , 298 K).



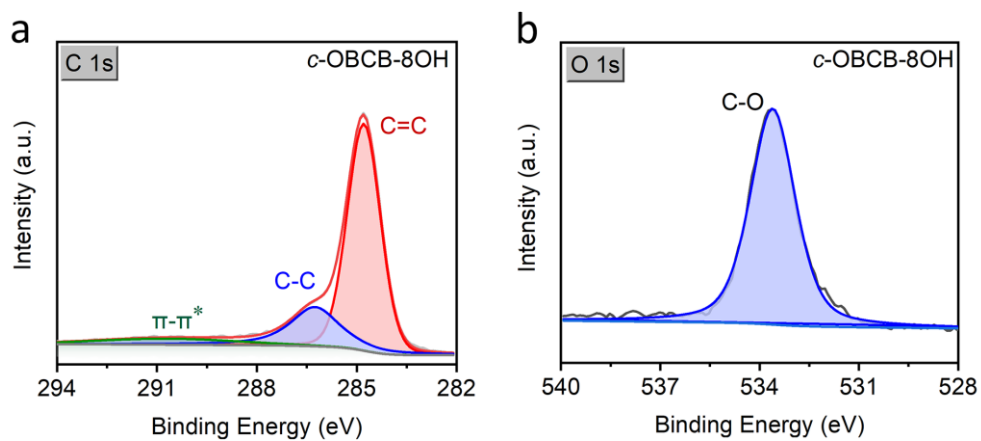
**Figure S14.** TGA plots of (a) *c*-HBC-8OH and (b) *c*-OBCB-8OH with a heating rate of  $10\text{ }^{\circ}\text{C min}^{-1}$  under air atmosphere.



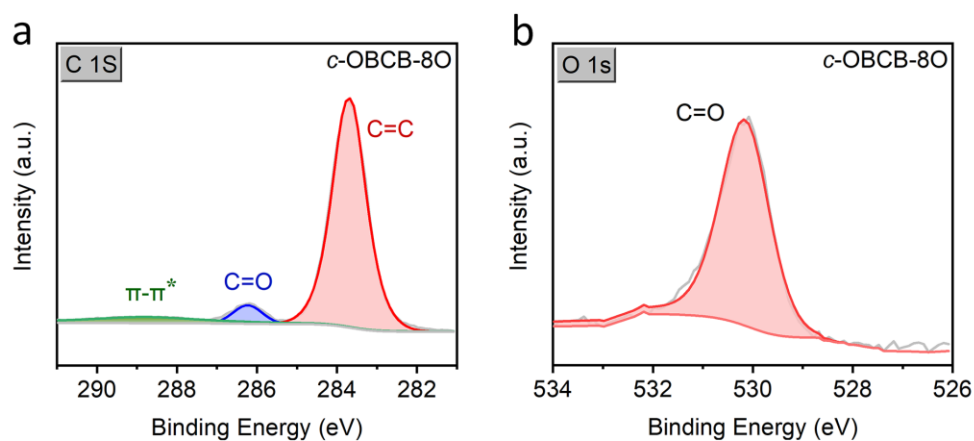
**Figure S15.** FT-IR spectra of *c*-OBCB-8OH and *c*-OBCB-8O.



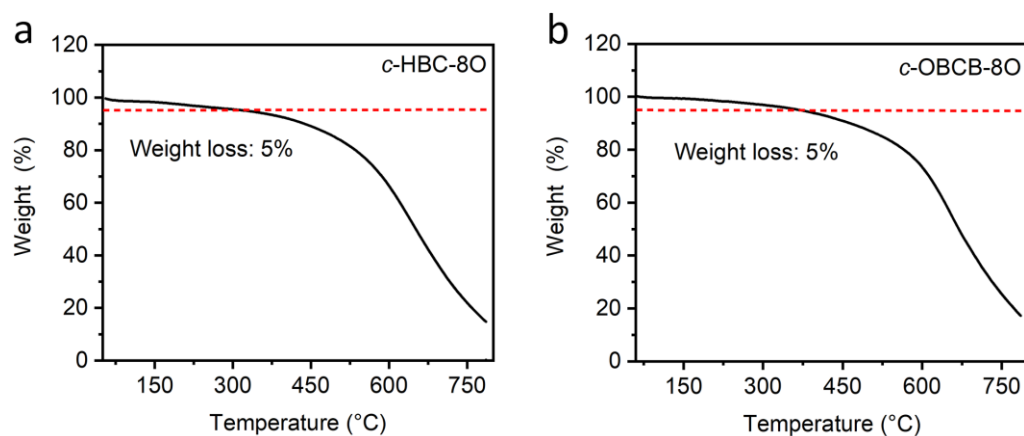
**Figure S16.** (a) C 1s and (b) O 1s XPS spectra of *c*-HBC-8OH.



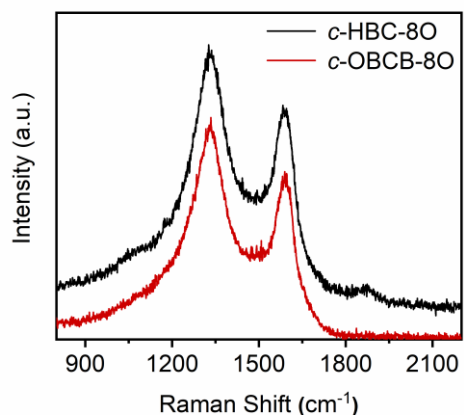
**Figure S17.** (a) C 1s and (b) O 1s XPS spectra of *c*-OBCB-8OH.



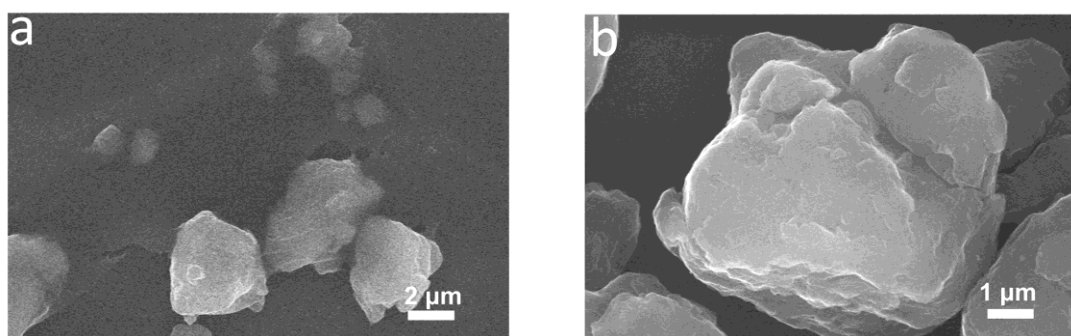
**Figure S18.** (a) C 1s and (b) O 1s XPS spectra of *c*-OBCB-8O.



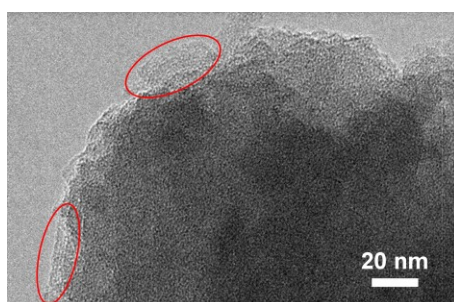
**Figure S19.** TGA plots of (a) *c*-HBC-8O and (b) *c*-OBCB-8O with a heating rate of 10 °C min<sup>-1</sup> under argon atmosphere.



**Figure S20.** The Raman spectra of the *c*-HBC-80 and *c*-OBCB-80.

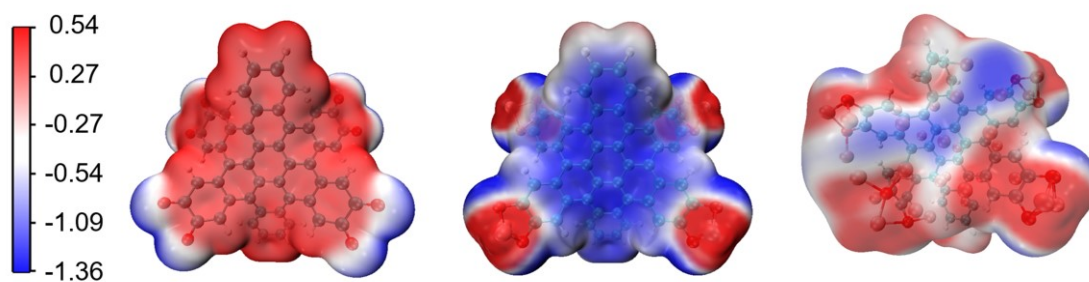


**Figure S21.** SEM images of *c*-OBCB-80.

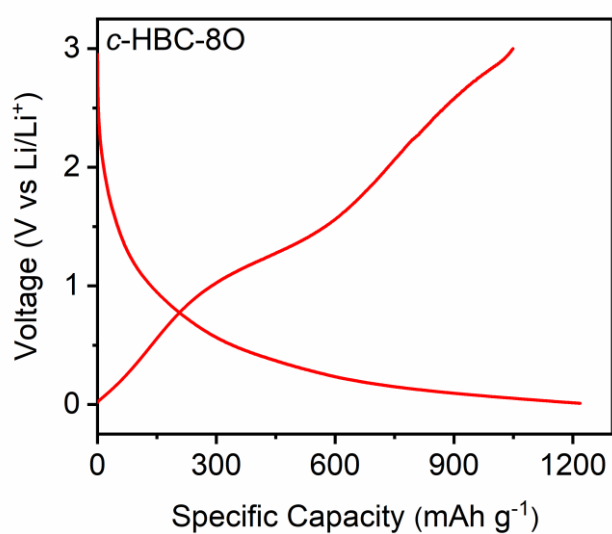


**Figure S22.** TEM image of *c*-OBCB-80.

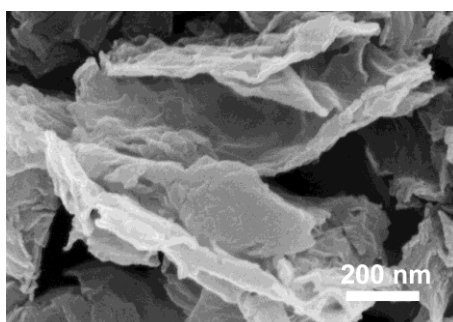




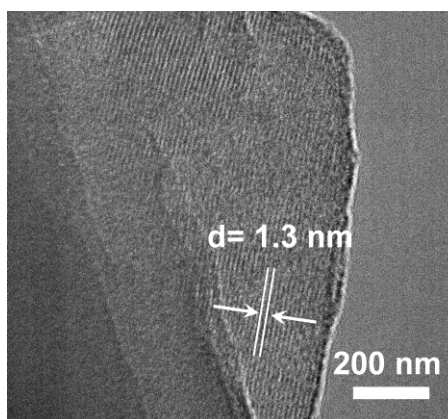
**Figure S23.** Distribution of ESP of *c*-HBC-80 in different states.



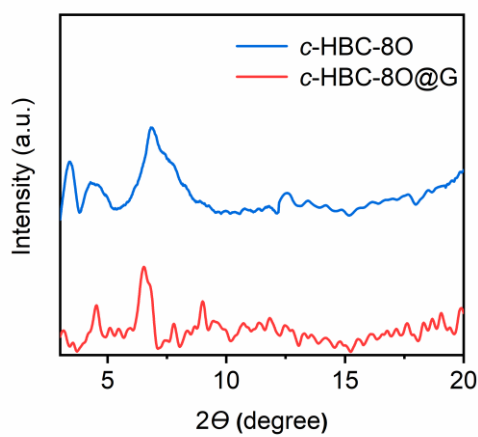
**Figure S24.** The charge and discharge curves of the second circle of *c*-HBC-80 at 50  $\text{mAh g}^{-1}$ .



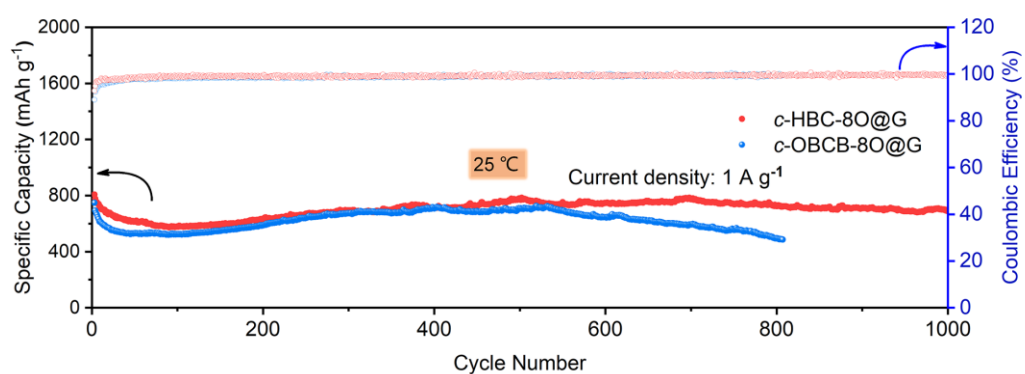
**Figure S25.** SEM image of *c*-HBC-80@G.



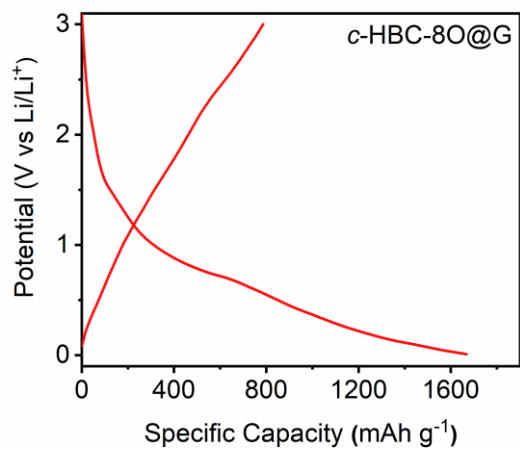
**Figure S26.** TEM image of *c*-HBC-80@G.



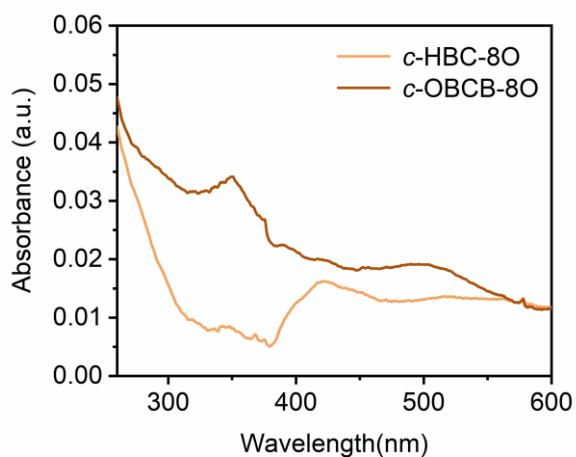
**Figure S27.** PXRD patterns of *c*-HBC-80 and *c*-HBC-80@G.



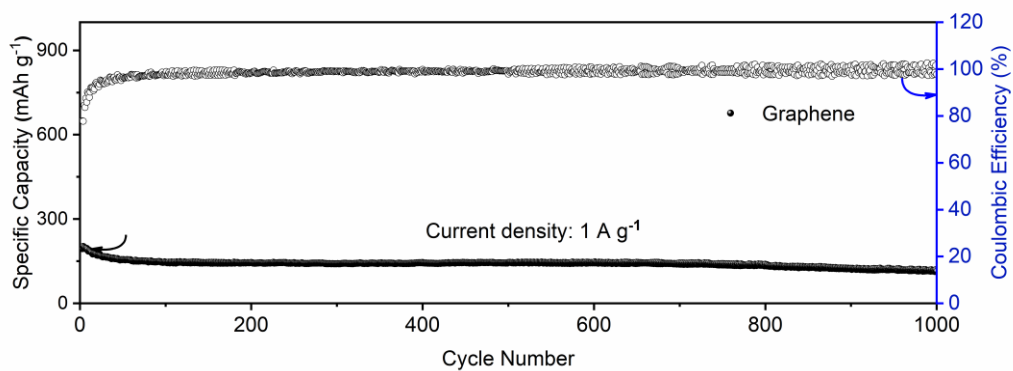
**Figure S28.** Cycling performance of *c*-HBC-80@G and *c*-OBCB-80@G at  $1 \text{ A g}^{-1}$  at  $25^\circ\text{C}$ .



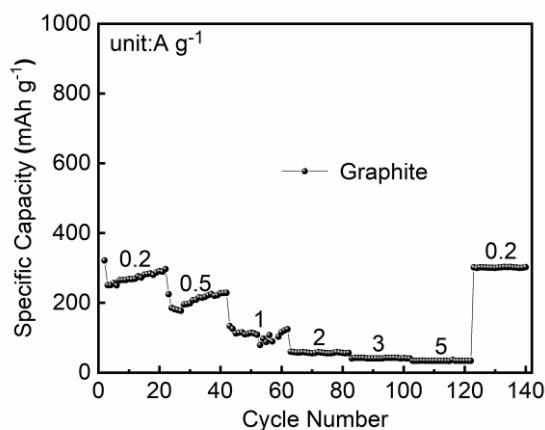
**Figure S29** The initial discharge and charge plots of c-HBC-80@G at 1 A g<sup>-1</sup>



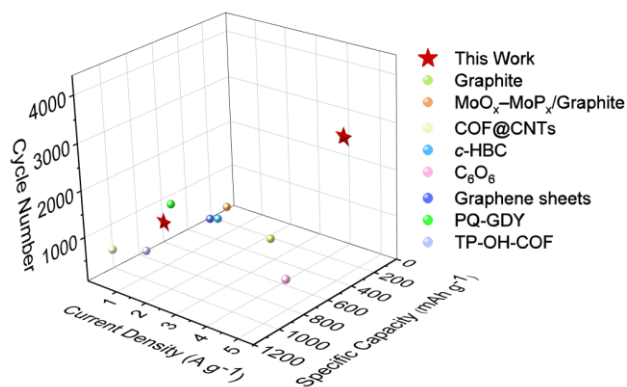
**Figure S30.** UV-vis spectra of c-HBC-80 and c-OBCB-80 saturated in EC: DMC= 1:1 mixed solution.



**Figure S31.** Cycling performance of graphene.



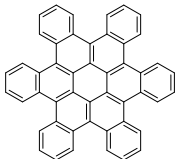
**Figure S32.** Rate performance of graphite anode at 25 °C.

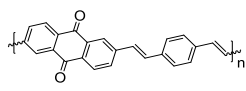


**Figure S33.** Comparisons of cycling performances and specific capacities between *c*-HBC-80@G and other typical anode materials.

**Table S1.** Comparisons of the electrochemical performance between *c*-HBC-80@G anodes and various other advanced anodes.

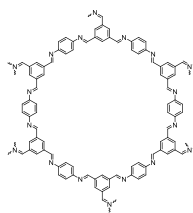
Samples	Current density (A g <sup>-1</sup> )	Specific capacity (mAh g <sup>-1</sup> )	Cycle number	Temperature (°C)	Ref.
<i>c</i> -HBC-80	1	808.0	1000	25	This work
<i>c</i> -HBC-80	5	298.3	3000	25	This work
<i>c</i> -HBC-80	0.2	270	1000	-20	This work

<b>Graphite</b>	2.232	236.8	100	25	7
<b>Graphite oxide frameworks (GOF)</b>	3	370	3500	25	8
<b>3D Crumpled graphene</b>	0.1	305	300	25	9
<b>Pyrazinoquinoxaline-based graphdiyne(PQ-GDY)</b>	0.2	570	900	25	10
<b>MoO<sub>x</sub> –MoP<sub>x</sub> /Graphite</b>	372	150	300	25	11
<b>Holey-Graphene</b>	2.232	320	100	25	12
<b>Graphene sheets</b>	0.05	221	50	25	13
<b>Graphite@CNT</b>	1.488	350	500	25	14
<b>Graphite@FeCl<sub>3</sub></b>	0.1	500	400	25	15
<b>Vertical graphene sheets</b>	372	456	400	25	16
<b>Multi-layer graphene fibers</b>	0.1	392	100	25	17
<b>Graphene oxide</b>	0.0525	917	100	25	18
<b>Graphdiyne</b>	3.6	342	4000	25	19
<b>Graphdiyne</b>	2.4	100	21500	-10	19
<b>C<sub>6</sub>O<sub>6</sub></b>	5	700	814	25	20
<b>Cyclized Polyacrylonitrile</b>	1	1090	810	25	21
	0.4	150	236	25	22
<b>c-HBC</b>					



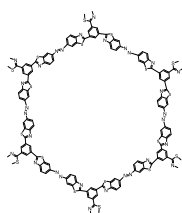
**PIAQ**

1      1000      486      25      23



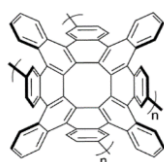
**COF@CNTs**

0.1      500      1021      25      24

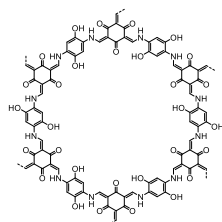


**AZO-1**

2.4      1000      75      25      25

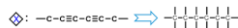
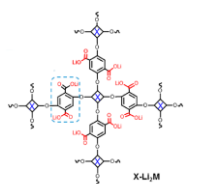


0.1      200      546      25      26

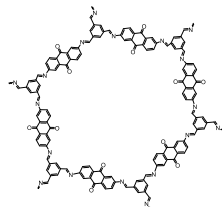


**TP-OH-COF**

0.1      764.1      100      25      27

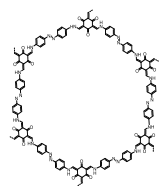


0.15      100      100      25      28



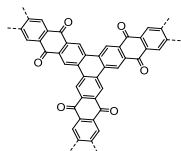
**DAAQ-COF**

1      787      500      25      29



1                    305.97                    3000                    25                    30

**TP-Azo-COF**



1                    95.8                    1500                    25                    31

**BQbTPL**

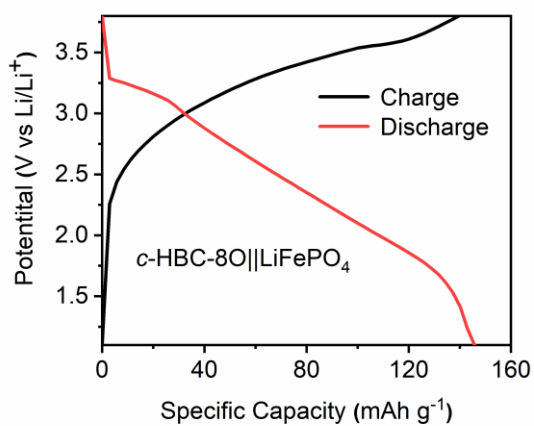


**Figure S34.** Charge and discharge curves of *c*-HBC-80@G || LiFePO<sub>4</sub> full cell at 1 C.

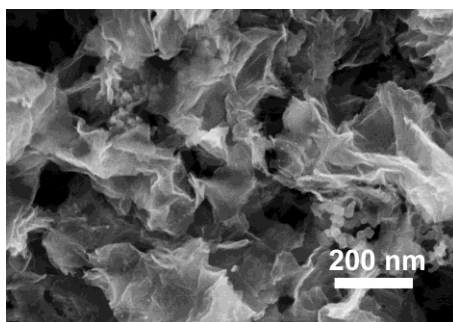


**Figure S35.** SEM image of the initial *c*-HBC-80 electrode.

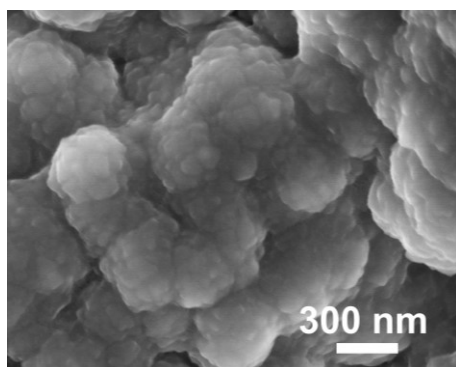


**Figure S36.** SEM image of *c*-HBC-80@G electrode surface after cycling.

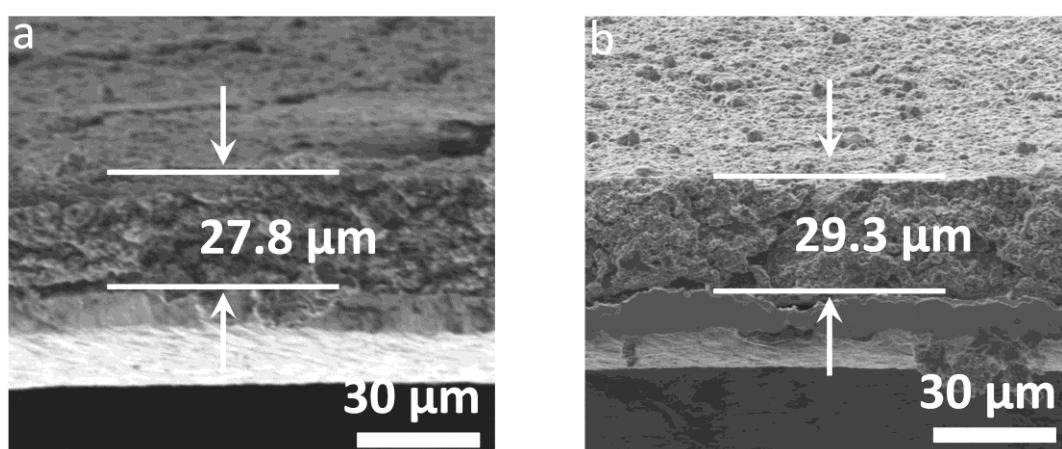


**Figure S37.** Cross section SEM images of *c*-HBC-80@G electrode (a) before and (b) after rate test.

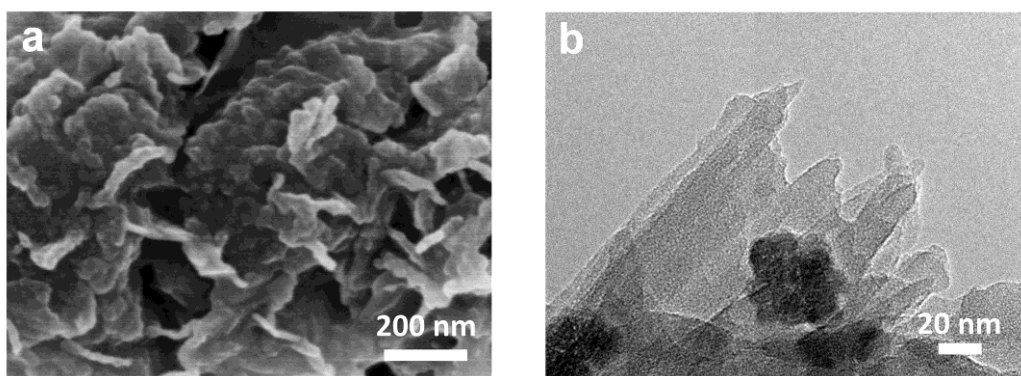


**Figure S38.** (a) SEM and (b) TEM images of *c*-HBC-80@G after 100 cycles at 100 mAh g<sup>-1</sup> under -20 °C.



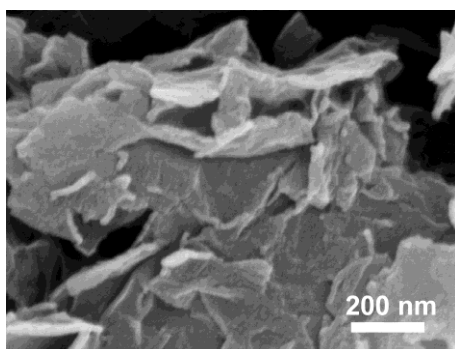


Figure S39. SEM image of c-OBCB-80@G.

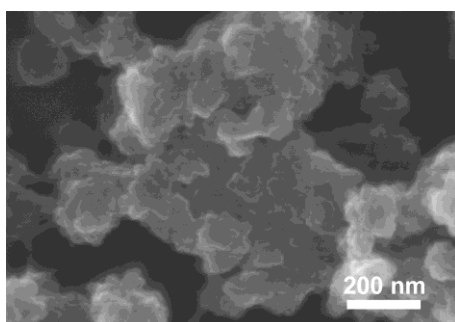


Figure S40. SEM image of c-OBCB-80@G after 140 cycles of rate test.

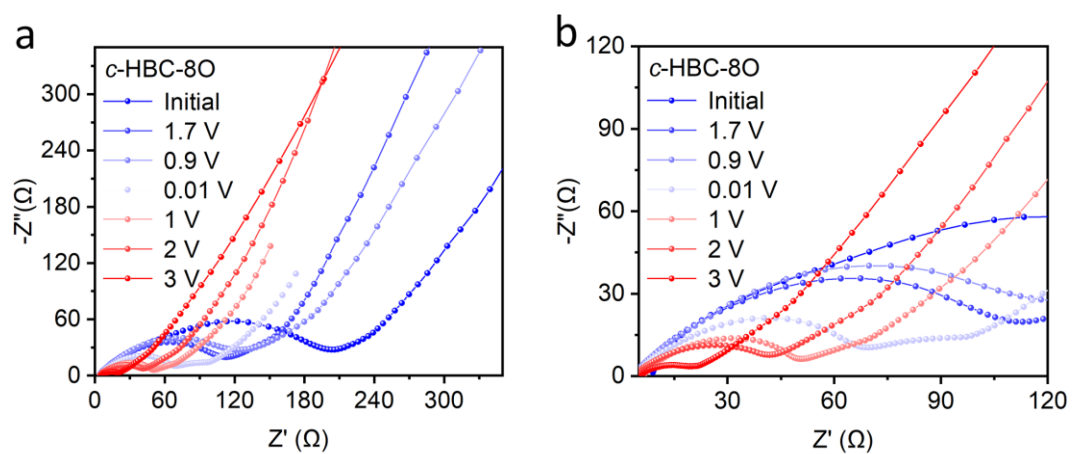
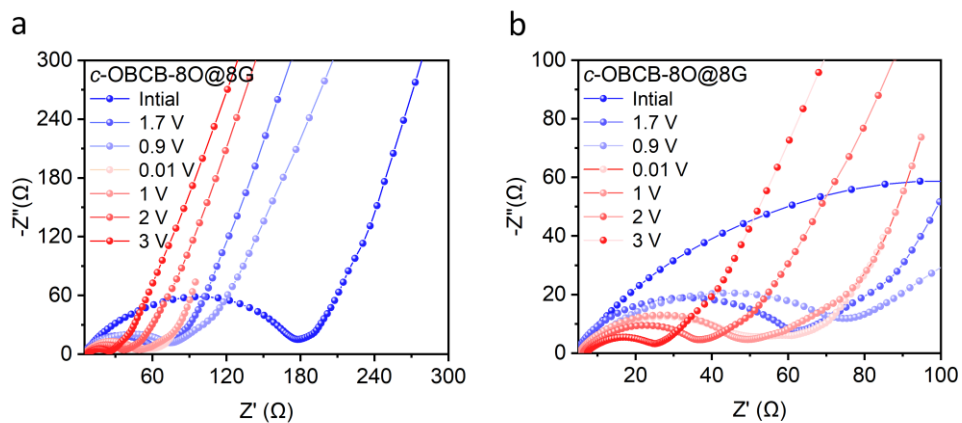
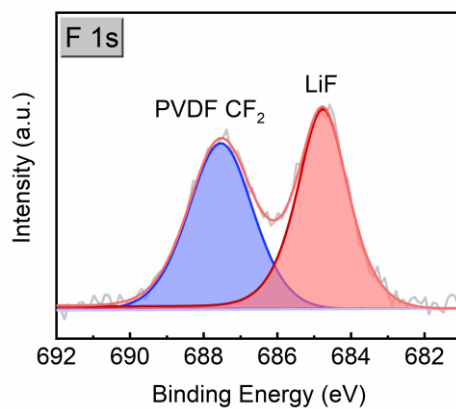


Figure S41. Nyquist pots of c-HBC-8O electrodes taken at different charge states.



**Figure S42.** Nyquist pots of *c*-OBCB-8O electrodes taken at different charge states.



**Figure S43.** F1s XPS spectra of the SEI of *c*-HBC-8O@G anodes.

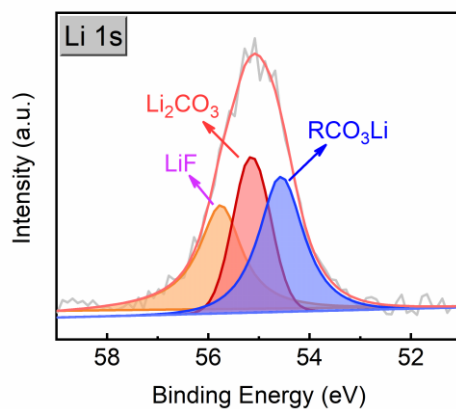


**Figure S44.** Li 1s XPS spectra of the SEI of *c*-HBC-8O@G anodes.

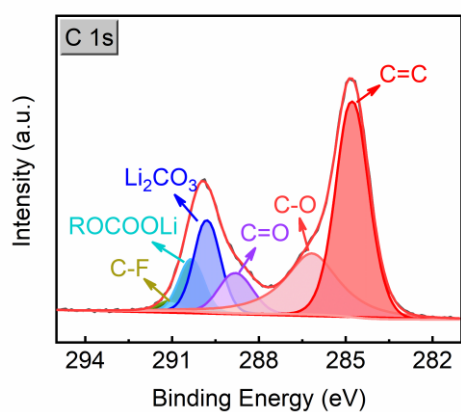


**Figure S45.** C1s XPS spectra of the SEI of *c*-HBC-80@G anodes.

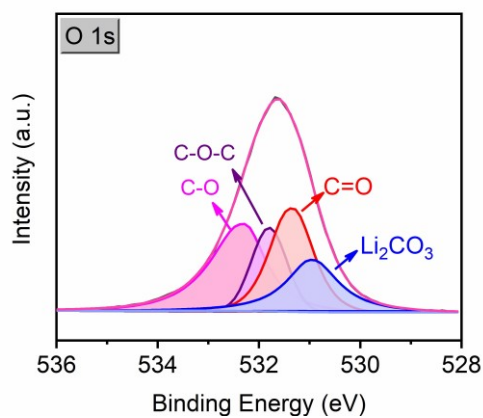


**Figure S46.** O1s XPS spectra of the SEI of *c*-HBC-80@G anodes.

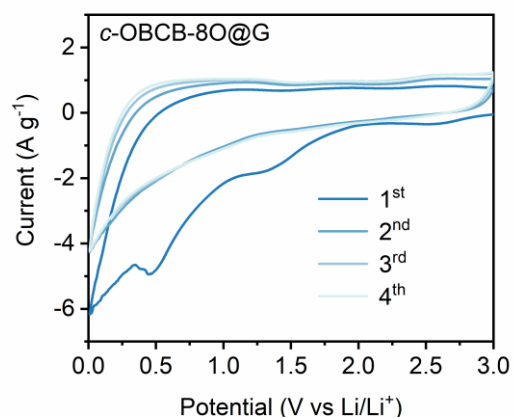


**Figure S47.** CV curves of *c*-OBCB-80 electrode at  $0.5 \text{ mV s}^{-1}$ .

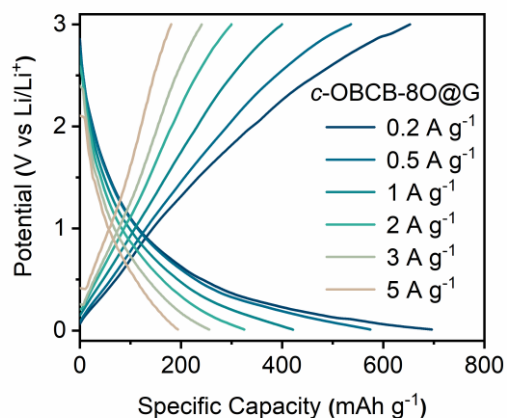


**Figure S48.** Charge and discharge curves of *c*-HBC-80 at various current densities.

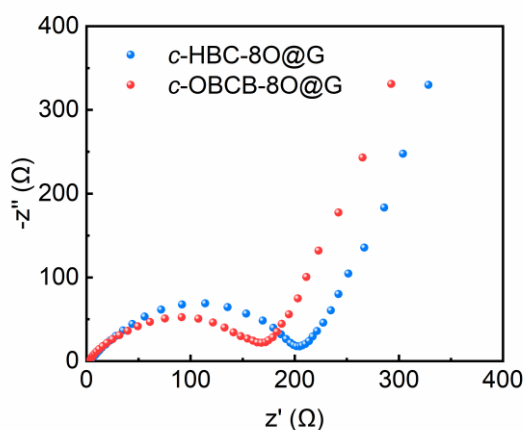


**Figure S49.** Electrochemical impedance spectroscopy (ESI) plots of *c*-HBC-80@G and *c*-OBCB-80@G.

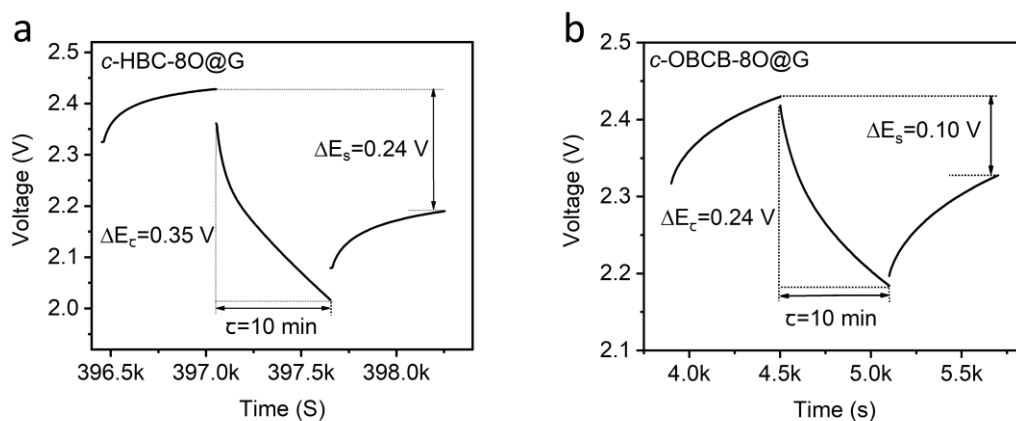


**Figure S50.** The single titration during GITT measurement of (a) *c*-HBC-80 and (b) *c*-OBCB-80 with representation of different parameters.

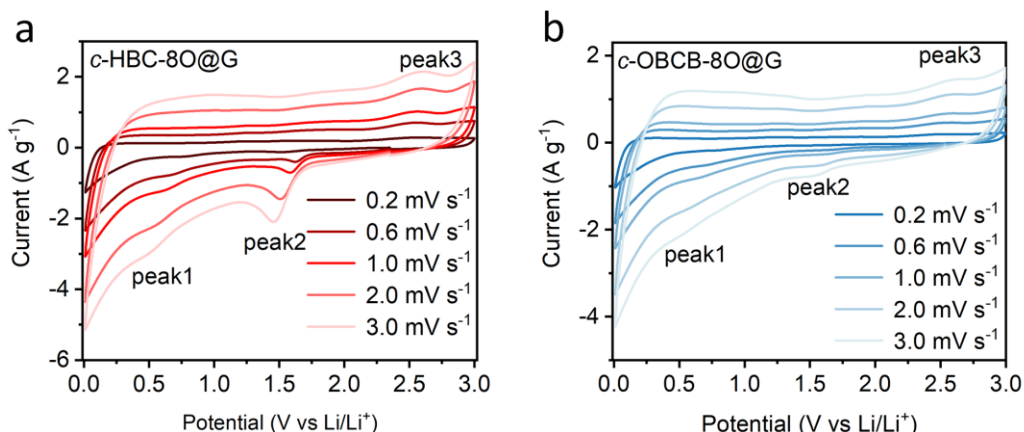


**Figure S51.** CV profiles of (a) *c*-HBC-80 and (b) *c*-OBCB-80 at different scan rates.

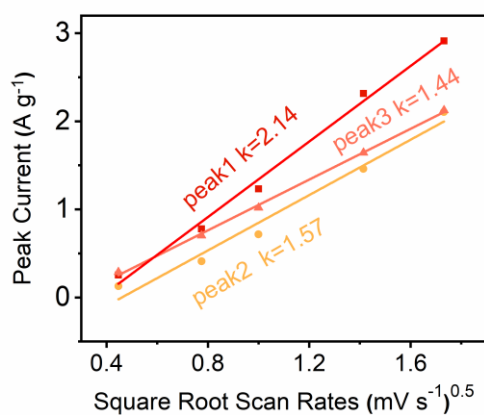


**Figure S52.** Corresponding relationship between the square root of the scan rate  $V^{1/2}$  and the peak current  $i_p$ .

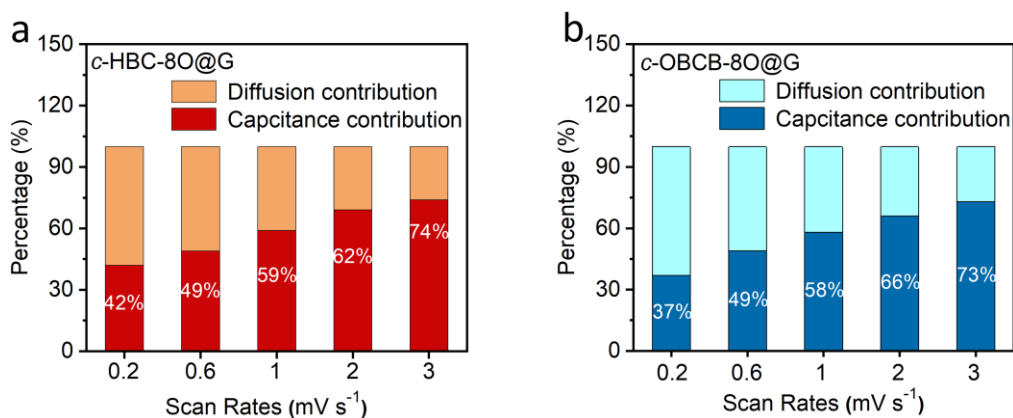


**Figure S53.** Capacitive contribution and diffusion currents of (a) *c*-HBC-80@G and (b) *c*-OBCB-80@G at different scan rates.

## References

1. M. J. Frisch, G. W. Trucks, H. B. Schlegel, G. E. Scuseria, M. A. Robb, J. R. Cheeseman, G. Scalmani, V. Barone, G. A. Petersson, H. Nakatsuji, X. Li, M. Caricato, A. V. Marenich, J. Bloino, B. G. Janesko, R. Gomperts, B. Mennucci, H. P. Hratchian, J. V. Ortiz, A. F. Izmaylov, J. L. Sonnenberg, Williams, F. Ding, F. Lipparini, F. Egidi, J. Goings, B. Peng, A. Petrone, T. Henderson, D. Ranasinghe, V. G. Zakrzewski, J. Gao, N. Rega, G. Zheng, W. Liang, M. Hada, M. Ehara, K. Toyota, R. Fukuda, J. Hasegawa, M. Ishida, T. Nakajima, Y. Honda, O. Kitao, H. Nakai, T. Vreven, K. Throssell, J. A. Montgomery Jr., J. E. Peralta, F. Ogliaro, M. J. Bearpark, J. J. Heyd, E. N. Brothers, K. N. Kudin, V. N. Staroverov, T. A. Keith, R. Kobayashi, J. Normand, K. Raghavachari, A. P. Rendell, J. C. Burant, S. S. Iyengar, J. Tomasi, M. Cossi, J. M. Millam, M. Klene, C. Adamo, R. Cammi, J. W. Ochterski, R. L. Martin, K. Morokuma, O. Farkas, J. B. Foresman and D. J. Fox, *Journal*, 2016.
2. C. Lee, W. Yang and R. G. Parr, *Phys Rev B Condens Matter*, 1988, **37**, 785-789.
3. CYLview20; Legault, C. Y., Université de Sherbrooke, 2020 (<http://www.cylview.org>).
4. A. D. William Humphrey, Klaus Schulten, *J. Mol. Graph. Model*, 1996, **14**, 33-38.
5. T. Liu, C. Qi, Q. Zhou, W. Dai, Y. Lan, L. Xu, J. Ren, Y. Pan, L. Yang, Y. Ge, Y. K. Qu, W. Li, H. Li and S. Xiao, *Org. Lett.*, 2022, **24**, 472-477.
6. S. Xiao, S. J. Kang, Y. Wu, S. Ahn, J. B. Kim, Y.-L. Loo, T. Siegrist, M. L. Steigerwald, H. Li and C. Nuckolls, *Chem. Sci.*, 2013, **4**, 2018-2023.
7. K. H. Chen, V. Goel, M. J. Namkoong, M. Wied, S. Müller, V. Wood, J. Sakamoto, K. Thornton and N. P. Dasgupta, *Adv. Energy Mater.*, 2020, **11**, 2003336.
8. J. Lee, C. Kim, J. Y. Cheong and I.-D. Kim, *Chem*, 2022, **8**, 2393-2409.
9. M. J. Lee, K. Lee, J. Lim, M. Li, S. Noda, S. J. Kwon, B. DeMattia, B. Lee and S. W. Lee, *Adv. Funct. Mater.*, 2021, **31**, 2009397.
10. L. Gao, X. Ge, Z. Zuo, F. Wang, X. Liu, M. Lv, S. Shi, L. Xu, T. Liu, Q. Zhou, X. Ye and S. Xiao, *Nano Lett.*, 2020, **20**, 7333-7341.
11. S. M. Lee, J. Kim, J. Moon, K. N. Jung, J. H. Kim, G. J. Park, J. H. Choi, D. Y. Rhee, J. S. Kim, J. W. Lee and M. S. Park, *Nat. Commun.*, 2021, **12**, 39.
12. Q. Cheng, R. Yuge, K. Nakahara, N. Tamura and S. Miyamoto, *J. Power Sources*, 2015, **284**, 258-263.
13. H. F. Xiang, Z. D. Li, K. Xie, J. Z. Jiang, J. J. Chen, P. C. Lian, J. S. Wu, Y. Yu and H. H. Wang, *RSC Adv.*, 2012, **2**, 6792-6799.
14. J. Xu, X. Wang, N. Yuan, B. Hu, J. Ding and S. Ge, *J. Power Sources*, 2019, **430**, 74-79.
15. F. Wang, J. Yi, Y. Wang, C. Wang, J. Wang and Y. Xia, *Adv. Energy Mater.*, 2014, **4**, 1300600.
16. Y. Mu, M. Han, J. Li, J. Liang and J. Yu, *Carbon*, 2021, **173**, 477-484.

17. G. Wang, S. Zhang, X. Li, X. Liu, H. Wang and J. Bai, *Electrochim. Acta*, 2018, **259**, 702-710.
18. Y. Sun, J. Tang, K. Zhang, J. Yuan, J. Li, D. M. Zhu, K. Ozawa and L. C. Qin, *Nanoscale*, 2017, **9**, 2585-2595.
19. J. An, H. Zhang, L. Qi, G. Li and Y. Li, *Angew. Chem. Int. Ed.*, 2022, **61**, e202113313.
20. J. L. Sha Li, Yimiao Zhang, Shilin Zhang, Tao Jiang, Zhongli Hu, Junjie Liu, De-Yin Wu, Li Zhang, Zhongqun Tian, *Adv. Energy Mater.*, 2022, 2201347.
21. W. Zhang, M. Sun, J. Yin, E. Abou-Hamad, U. Schwingenschlogl, P. Costa and H. N. Alshareef, *Angew. Chem. Int. Ed.*, 2021, **60**, 1355-1363.
22. J. Park, C. W. Lee, S. H. Joo, J. H. Park, C. Hwang, H.-K. Song, Y. S. Park, S. K. Kwak, S. Ahn and S. J. Kang, *J. Mater. Chem. A*, 2018, **6**, 12589-12597.
23. Z. Man, P. Li, D. Zhou, R. Zang, S. Wang, P. Li, S. Liu, X. Li, Y. Wu, X. Liang and G. Wang, *J. Mater. Chem. A*, 2019, **7**, 2368-2375.
24. Z. Lei, Q. Yang, Y. Xu, S. Guo, W. Sun, H. Liu, L.-P. Lv, Y. Zhang and Y. Wang, *Nat. Commun.*, 2018, **9**, 576.
25. V. Singh, J. Kim, B. Kang, J. Moon, S. Kim, W. Y. Kim and H. R. Byon, *Adv. Energy Mater.*, 2021, **11**, 2003735.
26. Y. Zhang, Y. Zhu, D. Lan, S. H. Pun, Z. Zhou, Z. Wei, Y. Wang, H. K. Lee, C. Lin, J. Wang, M. A. Petrukhina, Q. Li and Q. Miao, *J. Am. Chem. Soc.*, 2021, **143**, 5231-5238.
27. G. L. Lipeng Zhai, Xiubei Yang, Sodam Park, Diandian Han, Liwei Mi, Yanjie Wang, Zhongping Li, Sang-Young Lee, *Adv. Funct. Mater.*, 2021, **32**, 2108798.
28. S. Zhang, S. Ren, D. Han, M. Xiao, S. Wang, L. Sun and Y. Meng, *ACS Appl. Mater. Interfaces*, 2020, **12**, 36237-36246.
29. H. Zhao, H. Chen, C. Xu, Z. Li, B. Ding, H. Dou and X. Zhang, *ACS Appl. Energy Mater.*, 2021, **4**, 11377-11385.
30. G. Zhao, Y. Zhang, Z. Gao, H. Li, S. Liu, S. Cai, X. Yang, H. Guo and X. Sun, *ACS Energy Lett.*, 2020, **5**, 1022-1031.
31. Z. Ouyang, D. Tranca, Y. Zhao, Z. Chen, X. Fu, J. Zhu, G. Zhai, C. Ke, E. Kymakis and X. Zhuang, *ACS Appl. Mater. Interfaces*, 2021, **13**, 9064-9073.